International Journal of Nanomedicine

Dovepress
open access to scientific and medical research

Open Access Full Text Article

ORIGINAL RESEARCH

Anti-Tumor Efficacy of Oleuropein-Loaded ZnO/Au Mesoporous Silica Nanoparticle in 5-FU-Resistant Colorectal Cancer Cells

Sang Mi Park[1,2], Da Yeon Kim[3], Kyeong Hyeon Lee[1], Yong-Il Shin[1,4], Sang-Cheol Han[5], Sang-Mo Kwon[1,2]

[1]Department of Physiology, Laboratory of Vascular Medicine and Stem Cell Biology, School of Medicine, Pusan National University, Yangsan, Republic of Korea; [2]BK21 GRAND Convergence Medical Science Education Research Center, Pusan National University, Yangsan, South Korea; [3]Genetic & Epigenetic Toxicology Research Group, Korea Institute of Toxicology (KIT), Daejeon, Republic of Korea; [4]Department of Rehabilitation Medicine, Pusan National University Yangsan Hospital, Yangsan, Republic of Korea; [5]CEN Co., Ltd. Nanoconvergence Center, Muan-ro, Miryang, 761, Republic of Korea

Correspondence: Sang-Mo Kwon, Department of Physiology, Laboratory of Vascular Medicine and Stem Cell Biology, School of Medicine, Pusan National University, Yangsan, Republic of Korea, Tel +82-51-510-8072, Fax +82-51-510-8076, Email smkwon323@pusan.ac.kr

Purpose: 5-fluorouracil (5-FU) is a first-line chemotherapeutic agent used to treat colorectal cancer (CRC). However, 5-FU induces drug resistance and activation of cancer stem cells (CSCs). In the present study, we designed a novel biocompatible nanomedicine system with high efficacy and biocompatibility by synthesizing mesoporous silica nanoparticle (MSN)-structured ZnO and gold ions. Oleuropein (OLP) is a phenolic compound derived from olive leaves that exerts anti-cancer effects. Therefore, we synthesized OLP-loaded ZnO/Au MSNs (ZnO/Au/OLP MSNs) and examined their anti-cancer effects on 5-FU-resistant CRC cells.

Methods: ZnO/Au MSNs were synthesized and functionalized, and their physical and chemical compositions were characterized using UV-visible spectroscopy, dynamic light scattering, and transmission electron microscopy (TEM). Their effects were assessed in terms of cellular proliferation capacity, migration and invasion ability, colony-forming ability, spheroid-forming ability, reactive oxygen species (ROS) production, and mitochondrial membrane depolarization.

Results: ZnO/Au MSNs were mostly composed of various ions containing ZnO and gold ions, had a spheroid phenotype, and exhibited no cytotoxicity. ZnO/Au/OLP MSNs reduced cell viability and CSC formation and induced apoptosis of 5-FU-resistant CRC cells via necrosis via ROS accumulation and DNA fragmentation.

Conclusion: ZnO/Au/OLP MSNs exhibited anti-cancer activity by upregulating necrosis. These results revealed that ZnO/Au/OLP MSNs are a novel drug delivery system for 5-FU CRC therapy.

Keywords: gold nanoparticles, drug resistance, MSNs, AuNPs, colorectal cancer cell, oleuropein

Introduction

Colorectal cancer (CRC) is the third most common cause of cancer-related mortality worldwide, with more than 1.85 million cases and 850,000 deaths annually.[1] Chemotherapy is commonly used to treat patients with colorectal cancer. However, conventional chemotherapeutic agents have many side effects due to their toxicity to normal cells.[2] 5-Fluorouracil (5-FU) is a first-line treatment for CRC. However, its use has many limitations owing to the various side effects and drug resistance of cancer cells. The most common adverse effects include leukopenia, diarrhea, stomatitis, nausea, vomiting, and alopecia.[3]

Resistance to chemotherapy is a major hurdle in CRC treatment, often mediated through various cellular mechanisms. These include the overexpression of drug efflux pumps, alterations in drug targets, enhanced DNA repair mechanisms, and evasion of apoptosis. Key biomarkers linked to chemoresistance in CRC include the overexpression of the ABC transporters, mutations in KRAS and BRAF genes, and alterations in the TP53 and APC genes. These biomarkers are crucial in understanding the resistance pathways and targeting them therapeutically.

Received: 10 September 2023
Accepted: 29 February 2024
Published: 14 March 2024

Therefore, novel therapeutic systems targeting cancer cells with fewer side effects are required. Oleuropein (OLP), the main polyphenol in olive leaf extract, has shown anti-cancer effects against many types of cancer, including breast,[4] liver,[5] colorectal,[6–8] thyroid,[9] skin,[10] and lung cancers.[11] Accumulating evidence has shown that OLP reduces drug resistance in cancer cells. Upon treatment with oleuropein, the expression levels of p21, p53, and TNFRSF10B increase, whereas those of Bcl-2 and Mcl1 decrease in cisplatin-resistant ovarian cancers. In addition, OLP effectively reverses trastuzumab resistance in Tzb-resistant breast cancer cells via downregulation of HER2 expression.[12–14] In the context of CRC, previous studies have highlighted OLP's potential in targeting pathways implicated in cancer cell survival and proliferation, making it a promising candidate for overcoming 5-FU resistance.

In our research, we also discovered that OLP exerts anti-cancer effects on 5-FU-resistant CRC cells primarily through the induction of mitochondrial superoxide production and mitochondrial fragmentation.[15] To enhance the delivery and efficacy of OLP, we developed a novel delivery system using Mesoporous Silica Nanoparticles (MSNs). MSNs have several attractive features for application as novel drug delivery systems, such as large surface areas, tailorable pore sizes, and controllable particle sizes and shapes. The development of MSN-based delivery systems that can be used in both cancer diagnosis and treatment has attracted tremendous interest in the past decade. MSN-based delivery systems improve therapeutic efficacy and reduce cytotoxicity in normal tissue.[16–18] To enhance the delivery and efficacy of OLP to 5-FU-resistant CRC cells, we used ZnO/Au MSNs. Our approach utilizes ZnO/Au MSNs, which are composed mainly of Au and Zn ions and have a spherical structures with reduced ionicity; thus, they have a long shelf life and stability with no deterioration or rancidity. The Food and Drug Administration (FDA) approved nanoparticles that exert effective anti-cancer effects at a concentration of approximately 10% of the contained drugs.[19] In this research, ZnO/Au/OLP MSNs contain 20% (w/w) OLP.

Here, the anti-cancer effect of the ZnO/Au/OLP MSNs was confirmed. The results of the present study demonstrated the suppressive effect of ZnO/Au/OLP MSNs on 5-FU-resistant CRC cells via mitochondria-mediated apoptosis. Treatment with ZnO/Au/OLP MSNs suppressed the function of 5-FU-resistant CRC cells and promoted late-phase of apoptosis. Notably, ZnO/Au/OLP MSNs significantly induced intracellular ROS accumulation and the loss of mitochondrial membrane potential. Overall, these findings suggest that ZnO/Au/OLP MSNs have the potential to be a novel therapeutic strategy for patients with 5-FU-resistant CRC.

Materials and Methods

Synthesis of MSNs

1. In Group A, CTAB (0.5 g) was dissolved in DI water, followed by the addition of 2 mL of 1 M NaOH. The resultant solution was maintained at 60°C with stirring.
2. Concurrently, 1 mL of TEOS was dissolved in 5 mL of methanol to form Group B, whereas TSD was added to 0.5 mL of ethanol to constitute Group C.
3. A total of 8 mL Group B was incrementally added to Group A with agitation and left to interact for 20 min. Subsequently, Group C and the residual volume of Group B were added and stirred for another 30 min.
4. The synthesized nanoparticles (NPs) were immersed in a 100 mL ethanol solution containing 0.3 g of ammonium nitrate and agitated at 60°C for several hours to facilitate CTAB extraction.
5. The harvested particles were rigorously washed with DI water and centrifuged. The sediment was washed with ethanol.
6. A 1:1 v/v mixture of TMB in ethanol and distilled water was then added to the NPs. This composite was autoclaved at 140°C for 4 days.

Synthesis of ZnO MSNs

The synthesis of Zinc Oxide (ZnO) Mesoporous Silica Nanoparticles (MSNs) was detailed in the Supplementary Figure 1.

1. Solution A was formulated by solubilizing 0.5 g CTAB in DI water, followed by the incremental addition of 2 mL of 1 M NaOH at 60°C.
2. Separately, a solution containing 1 mL of TEOS and AEAPTMS (0.1 g) in ethanol (at 1:5 volume and weight ratios) was prepared and integrated into Solution A, leading to the formation of a white precipitate.
3. The precipitate was subjected to filtration, rinsed, and then dried at 80°C for 48 h.
4. To eliminate CTAB, the dehydrated matter was dispersed in 100 mL ethanol, followed by the addition of 0.3 g NH_4NO_3. The admixture was stirred at 60°C for several hours, with the solid fraction being separated and dried at 60°C for 12 h.
5. To embed zinc, 0.2 g $ZnCl_2$ was dissolved in DI water, and the pre-prepared silica nanoparticles were integrated.
6. The resulting solution was then subjected to rotary evaporation, centrifugation, and sequential washing with water and ethanol. The purified product was desiccated at 80°C for 12 h.
7. Calcination was performed at 550°C for a period exceeding 5 h to obtain ZnO MSNs.

Synthesis of ZnO/Au MSNs

1. Ionized gold was formed by dissolving tetrachloroauric acid in DI water.
2. The gold ion solution was amalgamated with ZnO MSNs, producing a slurry.
3. Sodium hydroxide, which served as the reducing agent, was added, and the resultant admixture was agitated for 10 min.
4. After agitation, the solution was subjected to a 15-minute ultrasonication to ensure an optimal dispersion.
5. After ultrasonication, the solution was filtered and washed comprehensively with DI water.
6. The purified derivative was desiccated at 80°C for 6 h, yielding a pink-hued powder designated as ZnO/Au MSNs.

Synthesis of ZnO/Au/OLP MSNs (Oleuropein Loaded ZnO/Au MSNs)

The synthesis of Au/OLP loading of Zinc Oxide (ZnO) Mesoporous Silica Nanoparticles (MSNs) was detailed in the Supplementary Figure 2.

1. A total of 800 mg of MSNs were dissolved in DW and post-dissolution, ultrasonication was employed for 3 min to guarantee even dispersion.
2. Oleuropein (200 mg) was dissolved in DW and agitated at 300 RPM for 3 min.
3. Both solutions were combined and subjected to vacuum-induced depressurization, initially held at 70 BAR for 30 min and then reduced to 40 BAR for an additional 30 min.
4. After depressurization, the resulting mixture was air-dried under ambient conditions for 6 h.

Characterization of ZnO/Au MSNs

The morphology and structure of the ZnO/Au MSNs were analyzed using a Talos F200X transmission electron microscopy (TEM) device operated at an accelerating voltage of 200 kV. To prepare the samples, a droplet of the nanoparticle suspension was placed on a grid. This suspension was diluted in Milli-Q water (Millipore, USA) to achieve a concentration of 100 μg/mL. The excess liquid was gently blotted using filter paper, and the sample was air-dried before analysis. The elemental composition of the synthesized ZnO/Au MSNs was determined using energy-dispersive X-ray spectroscopy (EDS). Dynamic light scattering (DLS) measurements, encompassing the average diameter, poly-dispersity index, and ζ-potential of the nanoparticles, were conducted using a Zetasizer Nano ZSP (Malvern Instruments, Malvern, UK). UV-visible spectra of the ZnO/Au MSNs dispersions were obtained at room temperature using a UV-visible/NIR spectrophotometer (Jasco, V770). The dispersions were placed in a cuvette and their absorption spectra were recorded.

Cell Culture and Treatment Conditions

DLD-1 cells (KCLB 10221) were purchased from the American Type Culture Collection (ATCC, Manassas, VA, USA). The cells were maintained in RPMI-1640 (Gibco, Carlsbad, CA, USA) supplemented with 10% fetal bovine serum (FBS;

Gibco) and 1% penicillin-streptomycin in an atmosphere of 5% CO_2 at 37 °C. To establish a 5-FU-resistant stable DLD-1 cell line, DLD-1 cells were treated with 5 μM of 5-FU until they grew up to 80% confluency. The treatment killed most of the cells, and the surviving cells were passaged and maintained with 2 μM of 5-FU for 6 months. Resistance to 5-FU was confirmed by measuring cell viability after 5-FU treatment using CCK-8 assays. OLP and 5-FU were purchased from Sigma-Aldrich (St. Louis, MO, USA). The 5-FU compound was dissolved in distilled water, and 200 μM of OLP stock solution was prepared using dimethyl sulfoxide (DMSO).

Cell Viability Assay

The viability of cells was determined utilizing the D-Plus™ CCK cell viability assay kit (Dongin, LS, Korea). DLD-1 and DLD1/5FU cells (10,000 cells/well) were seeded in 96-well microplates and stabilized at 37 °C in a CO_2 incubator for 24 h. Serial drug dilutions were prepared using RPMI-1640 culture medium. Subsequently, varying concentrations of drug-containing medium were used to replace the original culture medium. After 72 h of incubation, cell viability was evaluated using a microplate reader (TECAN, Mannedorf, Switzerland) at an optical density (OD) of 450 nm. Relative viability was determined against vehicle ZnO/Au/OLP MSNs and a DMSO control, with sextuplicate measurements for precision.

BrdU Incorporation Assay

For 5-bromo-2′-deoxyuridine (Brd-U) incorporation assays, the Brd-U incorporation assay kit (Roche, United States) was used. The cells were seeded in 96-well cell culture plates at a density of 3×10^3 cells/well. After 24 h, the cells were incubated in RPMI-1640 media with DMSO, ZnO/Au MSNs, OLP, and ZnO/Au/OLP MSNs for 72 h. Next, the Brd-U–labeling solution (10 μM) was added to the cells, followed by a 3 h incubation. After DNA denaturation, peroxidase-labeled anti-BrdU monoclonal antibody was added to the cells, and the samples were incubated at room temperature for 90 min. The absorption of the Brd-U-antibody complexes was measured at the dual wavelengths of 450/595 nm.

Migration and Invasion Assay

For migration assays, the 8 μM pore Boyden chamber (Corning, NY, USA) was used. Cells were pre-treated with DMSO, ZnO/Au MSNs, OLP, and ZnO/Au/OLP MSNs for 72 h harvested and suspended in serum-free RPMI-1640 medium at a density of 5000 cells/100 μL, and then loaded into the upper chamber. In the bottom chamber, 500 μL of serum-containing culture medium was used to create a chemoattractant gradient. After 24 h, the migrated cells were fixed using 4% paraformaldehyde for 20 min at 25 °C, then stained with 0.5% crystal violet/25% methanol in PBS for 30 min at 25 °C, followed by thorough washing with tap water. The migrated cells were visualized using a Zeiss Axio Imager M2 optical microscope (Zeiss, Munich, Germany) and quantified using ImageJ software. The invasion assays were the same as the migration assays described in Materials and Methods.

Spheroid Formation Assay

The self-renewal ability of CSCs was assessed using tumorsphere formation assays. The 5-FU-resistant DLD-1 cells were dissociated into single cells and resuspended in CSC medium consisting of Dulbecco's modified Eagle's medium/nutrient mixture F-12 (DMEM/F12 (1:1); Gibco, Carlsbad, CA, USA) supplemented with B-27 (Thermo Fisher Scientific, Waltham, MA, USA), 20 ng/mL epidermal growth factor (EGF; Peprotech, Rocky Hill, NJ, USA), and 10 ng/mL basic fibroblast growth factor (bFGF Peprotech). Five hundred cells were seeded into ultra-low attachment 6-well plates in ultra-low attachment 24-well plates and maintained for up to 14 days. CSC medium was added twice per week. Fourteen days after seeding, the spheres were counted under a phase-contrast microscope, and their diameters were analyzed using ImageJ software (National Institutes of Health, Bethesda, MD, USA). To determine the probability of single cell-derived sphere formation, 10 cells/mL were seeded into 100 μL/well in 96-well microplates for 14 days. The sphere formation ability was observed under a microscope, and then illustrated and shown with the number of spheres and probability.

Soft Agar Assay

A soft agar assay was performed to detect anchorage-independent cell growth. First, the bottom agar was prepared with a 1:1 mixture of 1% agar (BD Difco, Franklin Lakes, NJ, USA) and 2X RPMI-1640 medium supplemented with 20% FBS (final conc. 0.5% agar, and 1X RPMI-1640 with 10% FBS). An aliquot of 1 mL of bottom base agar was poured into a 6-well plate

and allowed to solidify for 30 min at 25 °C. Top agar was prepared using a 1:1 mixture of 0.7% agar and 2X RPMI-1640 medium supplemented with 20% FBS (final conc. 0.35% agar, 1X RPMI-1640 with 10% FBS). Cells were harvested and resuspended at 50,000 cells/100 μL. A cell suspension of 100 μL was mixed with 1 mL of top agar, poured, and incubated at 37 °C CO_2 incubator for 14 days. Colonies were stained using 0.005% crystal violet for 2 h at 25 °C, then washed with distilled water twice and visualized. Images of the colonies were scanned and the colony number was quantified using ImageJ software.

Apoptosis Analysis

Annexin V FITC Apoptosis Detection Kit I (BD Biosciences, Franklin Lakes, NJ, USA) was used according to the manufacturer's instructions. Briefly, CSCs were dissociated into single cells, incubated with Annexin V-FITC antibody-containing buffer for 30 min in the dark, washed with cold PBS, and analyzed.

TUNEL Assay

Cells were detected using an In Situ Cell Death Kit (11684795910; Roche, Basel, Switzerland). Briefly, the cells were seeded on glass slides and treated with DMSO, ZnO/Au MSNs, OLP, and ZnO/Au/OLP MSNs for 72 h. The cells were fixed with 4% PFA for 30 min at room temperature and permeabilized with 0.1% Triton X-100 for 2 min on ice. The cells were then incubated with a TUNEL reaction mixture for 1 h at 37 °C and then counter-stained with DAPI for 10 min at room temperature. After incubation, the cells were mounted and counterstained with ProLongTM Diamond Antifade Mountant containing DAPI (Invitrogen P36962). The fluorescent signal was visualized using a Zeiss LSM 7000 confocal microscope (Zeiss, Munich, Germany).

JC-1 Assay

The mitochondrial membrane potential (MMP) was determined using a potential-sensitive fluorescent dye, JC-1 probe dye. The dual-emission probe changed color from red-orange to green as the mitochondrial membrane was depolarized. The JC-1 was loaded and incubated for 30 min at 37 °C. The results were visualized using a Lionheart FX automated microscope (BioTek, USA).

Western Blot Analysis

The cells were harvested and treated with PRO-PREP (iNtRON BIOTECHNOLOGY, 17081) for 30 min at 4 °C. The lysed cells were centrifuged at 13,000 rpm for 20 min at 4 °C, and protein concentration was calculated using Bicinchoninic Acid Assay Kit (Thermo Fisher Scientific, Waltham, 23227, MA, USA). The proteins were separated using 15% sodium dodecyl sulfate-polyacrylamide gel electrophoresis (SDS-PAGE) and transferred onto polyvinylidene difluoride membranes (Millipore, Billerica, MA, USA). The membrane was blocked with 5% skim milk in TBST for 40 min, and then treated with primary antibody and incubated overnight at 4 °C. For the primary antibodies, BAX (1:1000, Cell Signaling Technology, #2772S), NIX (1:1000, Cell Signaling Technology, #12396) and β-actin (1:5000, sc-47778) were used. Primary antibodies were detected using goat anti-mouse IgG-HRP (1:5000, Enzo Life Sciences, ADI-SAB -100-J, USA) or goat anti-rabbit IgG-HRP (1:5000, Enzo Life Sciences, AD I-SAB-300-J, USA). After the membrane was treated with Immobilon Crescendo Western HRP substrate (Millipore, WBLUR0500, USA), proteins were detected using an X-ray film or confirmed using an Amersham Imager 680 (GE Healthcare).

Statistical Analysis

Data, derived from a minimum of three individual experiments, are presented as mean ± SEM. The significance levels were categorized as follows: N.S. (not specified), N.D. (not determined), ** $P < 0.01$, and *** $P < 0.001$.

Results

Characterization of ZnO/Au MSNs

ZnO/Au MSNs and ZnO/Au/OLP MSNs were synthesized[20–22] and visualized by TEM (Figure 1A and B). The TEM analysis indicated that both types of nanoparticles were spherical. The average particle size of the ZnO/Au MSNs was 245.5 ± 1.8 nm, and for ZnO/Au/OLP MSNs, it was 240.5 ± 5.0 nm, as shown in Figure 1C. The average zeta potential

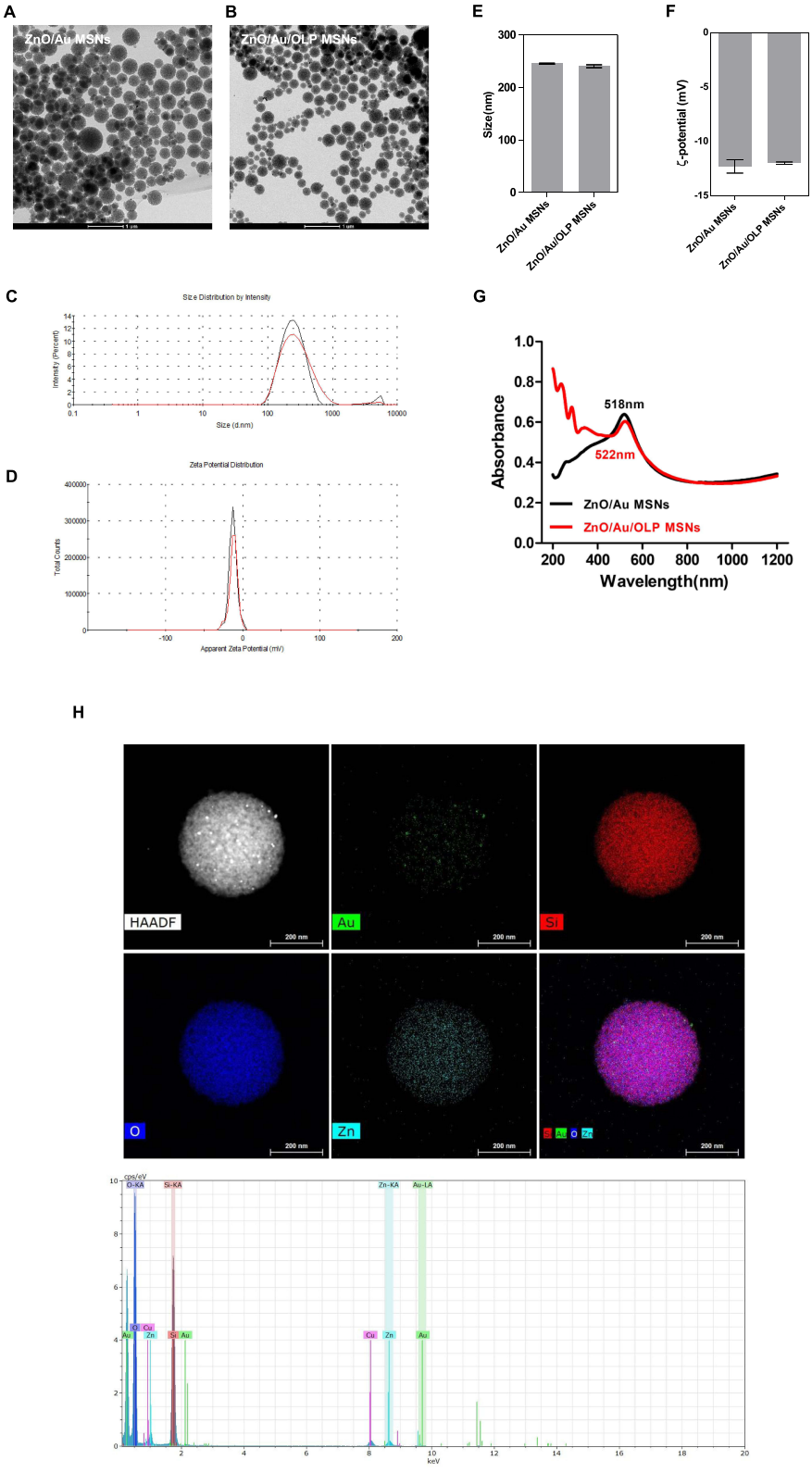

Figure 1 Characterization of ZnO/Au MSNs. (**A** and **B**) TEM images of ZnO/Au MSNs and ZnO/Au/OLP MSNs. (**C**) DLS size distribution histogram of ZnO/Au MSNs and ZnO/Au/OLP MSNs. (**D**) ζ-potential analysis of ZnO/Au MSNs and ZnO/Au/OLP MSNs. (**E** and **F**) Quantification data of (**C** and **D**). (**G**) Ultraviolet-visible (UV-vis) data of ZnO/Au MSNs and ZnO/Au/OLP MSNs(**H**) EDS analysis data of ZnO/Au MSNs.

for ZnO/Au MSNs and ZnO/Au/OLP MSNs was −12.3 ± 1.1 mV and −12.0 ± 0.2 mV, respectively, detailed in Figure 1D. Additionally, Figure 1E provides further quantitative analysis for the particle sizes of ZnO/Au MSNs and ZnO/Au/OLP MSNs, with the polydispersity index values being 0.198 ± 0.014 and 0.216 ± 0.024, respectively, indicating that the nanoparticles were highly monodispersed, as summarized in Table 2. The UV-vis spectrum of the ZnO/Au MSNs displayed a sharp absorption band centered at 518 nm, while the peak for the ZnO/Au/OLP MSNs shifted slightly to 522 nm after loading with OLP, depicted in Figure 1G. EDS mapping measurements, conducted to analyze the ions in the nanoparticles as shown in Figure 1H, and energy-dispersive X-ray spectroscopy (EDS) quantification analysis detailed in Table 1, reveal the elemental composition of the ZnO/Au MSNs. The presence of Si, Au, O, and Zn was confirmed with weight percentages of 41.61%, 0.75%, 53.58%, and 4.06%, respectively. The atomic percentages, also depicted in Table 1, provide additional insight into the stoichiometric distribution within the synthesized nanoparticles.

Anti-Proliferative Effects of ZnO/Au/OLP MSNs on 5-FU-Resistant CRC Cells

To evaluate ZnO/Au/OLP MSNs-induced anti-5-FU-resistant cancer effect, a 5-FU-resistant CRC cell line was established.[15] The IC50 value of the 5-FU-resistant CRC cell (37.74 μM) was approximately 6.95-fold higher than that of the parental CRC cells (5.43 μM) (Figure 2A). CCK-8 assays were performed to assess cell viability and evaluate the working concentrations of ZnO/Au/OLP MSNs and OLP. The viability of 5-FU-resistant CRC cells decreased in a dose-dependent manner after treatment with OLP (Figure 2B). In our study, the CCK-8 assay results indicated that the cells tolerated an OLP concentration of 100μM, maintaining 60–70% cell viability (Figure 2B). Similarly, a ZnO/Au/OLP MSNs concentration of 200μM was also tolerated by the cells, as evidenced by the 60–70% cell viability observed (Figure 2C). Based on these findings, we established the optimal concentrations for subsequent experiments: 100μM for OLP and 200μM for ZnO/Au/OLP MSNs. Notably, a solution of 200 μM ZnO/Au/OLP MSNs contained 40 μM OLP. We observed a dose-dependent decrease in the viability of 5-FU-resistant CRC cells when treated with ZnO/Au/OLP MSNs. In contrast, treatment with ZnO/Au MSN did not induce any significant change in cell viability (Figure 2C), suggesting that the ZnO/Au MSNs arebiocompatibility of ZnO/Au MSNs. Moreover, cell proliferation was confirmed using BrdU assays (Figure 2D). The BrdU assay results indicated that ZnO/Au/OLP inhibited the proliferation of 5-FU-resistant CRC cells compared to OLP alone. These results showed that ZnO/Au/OLP MSNs effectively reduced 5-FU-resistant CRC cell proliferation.

Inhibition of Migration and Invasion in 5-FU-Resistant DLD-1 Cells by ZnO/Au/OLP MSNs

Migration and invasion assays were performed to validate the migration and invasion abilities of 5-FU-resistant DLD-1 cells after treatment with ZnO/Au MSNs, ZnO/Au/OLP MSNs, and OLP (Figure 3A). The cells did not show any

Table 1 EDS Quantification Analysis

Element	Wt%	At%
Si	41.61	30.26
Au	0.75	0.08
O	53.58	68.40
Zn	4.06	1.27
Total	**100.00**	**100.00**

Table 2 Characterization of Nanoparticles

Nanoparticles	Size (nm)	Zeta Potential (mV)	PDI
ZnO/Au MSNs	245.5 ± 1.8	−12.3 ± 1.1	0.198 ± 0.014
ZnO/Au/OLP MSNs	240.5 ± 5.0	−12.0 ± 0.2	0.216 ± 0.024

Note: Data are expressed as mean ± SD (n = 3).

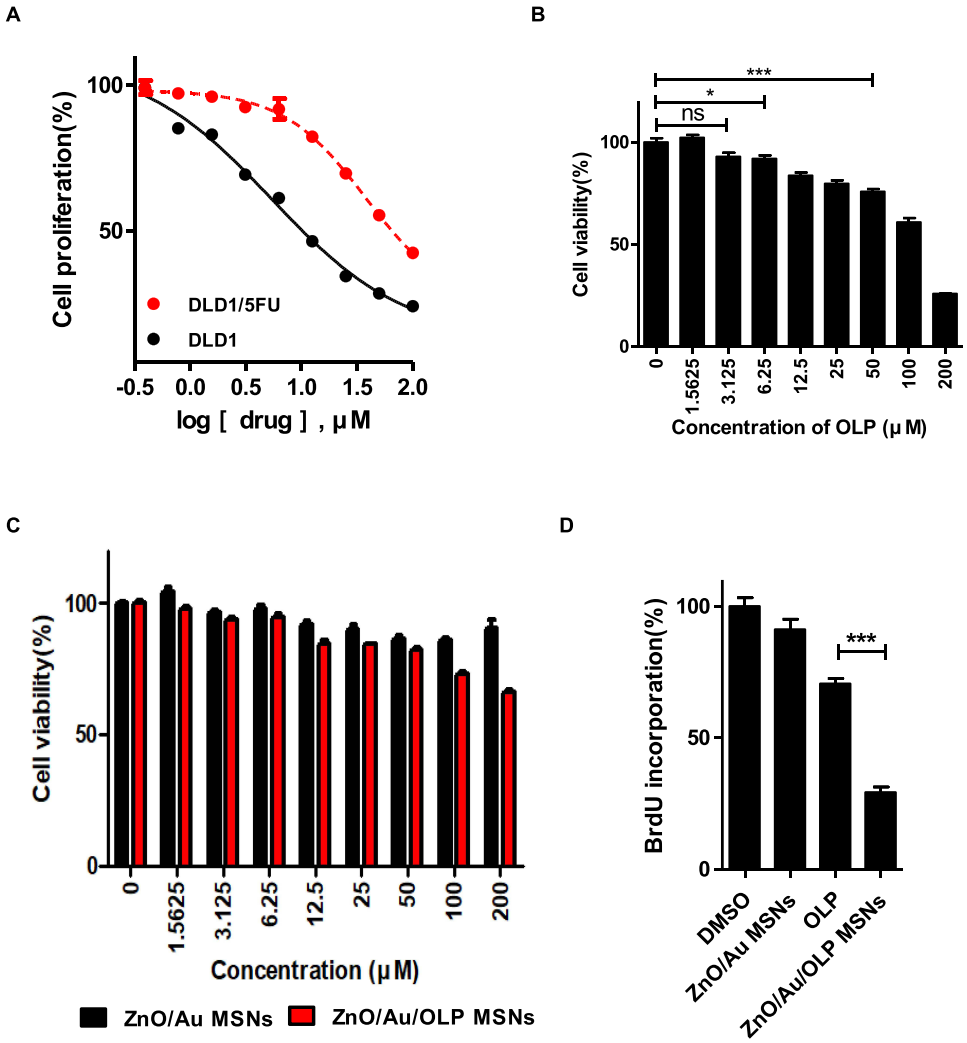

Figure 2 ZnO/Au/OLP MSNs and OLP decreased the proliferation of 5-FU-resistant CRC cells.(**A**) IC50 values of 5-FU on CRC cells, and 5-FU-resistant CRC cells determined using CCK-8 assays. (**B**) Cell viability was decreased in a dose-dependent manner after OLP treatment. (**C**) ZnO/Au MSNs did not influence 5-FU-resistant DLD-1 cells. However, ZnO/Au/OLP MSNs treatment reduced cell viability. (**D**) In Brd-U assays, OLP and ZnO/Au/OLP MSNs significantly reduced cell proliferation. Values are expressed as the mean ± standard error of the mean (S.E.M). ***p < 0.001 as compared to the control group.

migration ability after treatment with OLP or ZnO/Au/OLP MSNs (Figure 3B and C). Moreover, ZnO/Au/OLP MSNs caused a greater decrease in cell invasion than OLP MSNs (Figure 3C). These results indicate that ZnO/Au/OLP MSNs were more effective in reducing migration and invasion in 5- FU-resistant CRC cells compared to OLP treatment alone.

ZnO/Au/OLP MSNs Suppresses Colony and Sphere Forming Capacities

The colony formation ability of the 5-FU-resistant DLD-1 cells was suppressed following ZnO/Au/OLP MSNs and OLP treatment. Remarkably, there was a reduction in the colony-forming capability with ZnO/Au/OLP MSN treatment (Figure 4A and B). Both ZnO/Au/OLP MSNs and OLP treatments demonstrated an inhibitory effect on spheroid formation in 5-FU-resistant DLD-1 cells. Specifically, Figure 4C displays the morphology of the spheroids, illustrating the impact of these treatments. Notably, there was no significant difference in the number of spheroids between the OLP group and the ZnO/Au/OLP MSNs groups. However, the overall count was lower in the ZnO/Au/OLP MSNs group compared to the OLP group (Figure 4D). Additionally, Figure 4E focuses on the spheroid diameter, providing a comparison between the OLP aline group and the ZnO/Au/OLP MSNs group. A remarkable reduction in spheroid diameter was observed in the group treated with ZnO/Au/OLP MSNs, which aligns with the data observed in spheroid number and morphology. Next, the single cell-derived sphere-formation capability was evaluated. Interestingly, 22 of 24 wells were positive (91.7% sphere formation efficiency) for sphere formation in the DMSO control group. Moreover, the

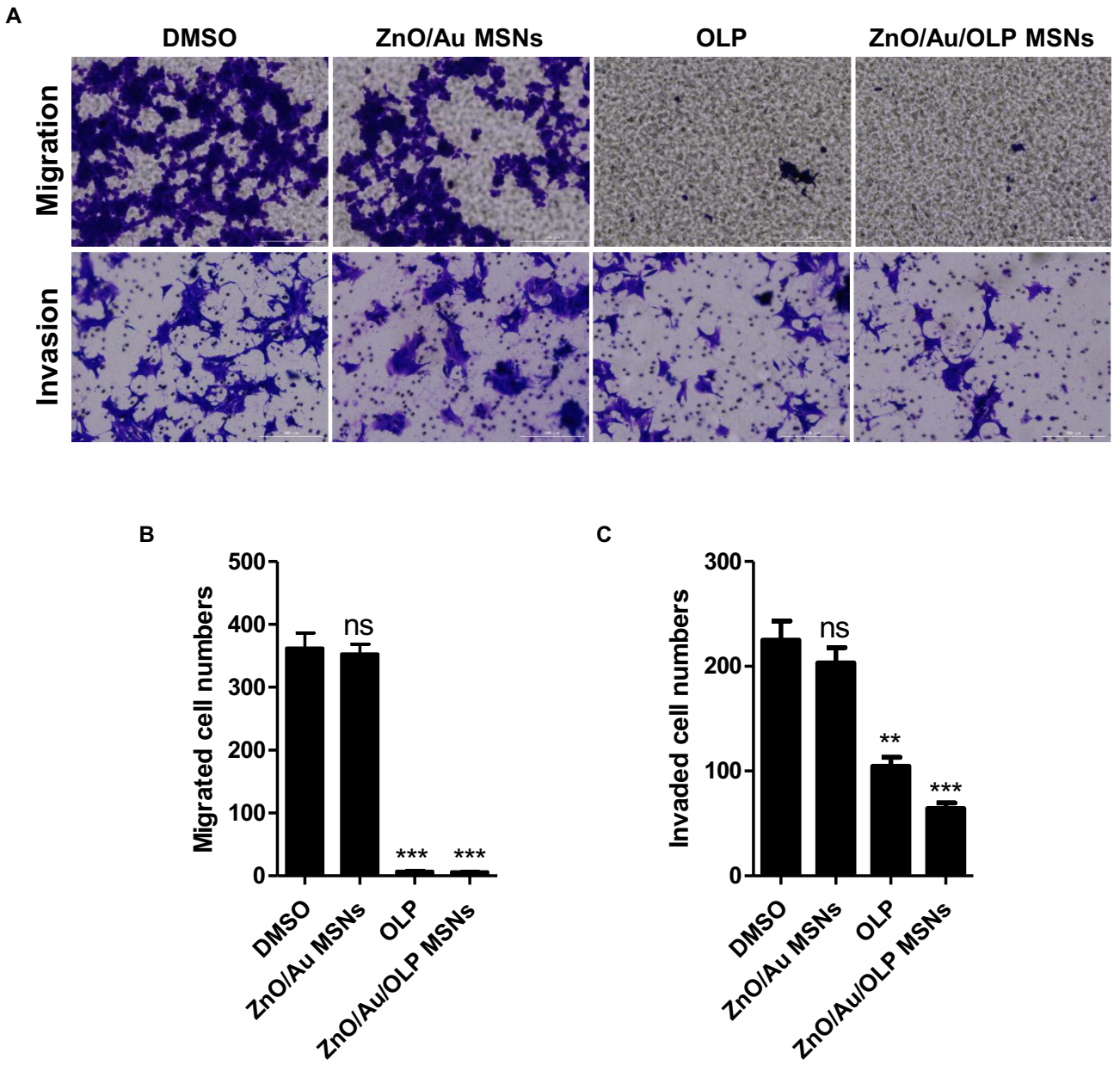

Figure 3 ZnO/Au/OLP MSNs significantly reduced 5-FU-resistant CRC cells' migration and invasion. Trans-well assays were used to measure the effects of OLP and ZnO/Au/OLP MSNs on cells' (**A**) migration and invasion. (**B** and **C**) Quantification data of migration and invasion. Values are expressed as mean ± standard error of the mean (S.E.M). **p < 0.01, ***p < 0.001 as compared to the control group.
Abbreviation: N.S, Not specified.

ZnO/Au MSN groups were positive (87.5% sphere formation efficiency). In contrast, the positive rates of sphere formation were drastically reduced at 200 μM OLP to 19/24 (79.2%), and 40 μM OLP containg ZnO/Au/OLP MSNs to 11/24 (45.8%), respectively (Figure 4F). Thus, these results showed that the colony- and spheroid-forming abilities were significantly reduced after ZnO/Au/OLP MSN treatment.

Induction of Apoptosis and ROS Accumulation in 5-FU-Resistant CRC Cells Treated with ZnO/Au/OLP MSNs

The apoptotic effects of ZnO/Au/OLP MSNs and OLP on 5-FU-resistant DLD-1 cells were evaluated using ANNEXIN V-PI staining as illustrated in Figure 5A. Apoptosis induction was further quantified through flow cytometry. The results indicated that the proportion of late apoptotic cells following treatment with either OLP or ZnO/Au/OLP MSNs was

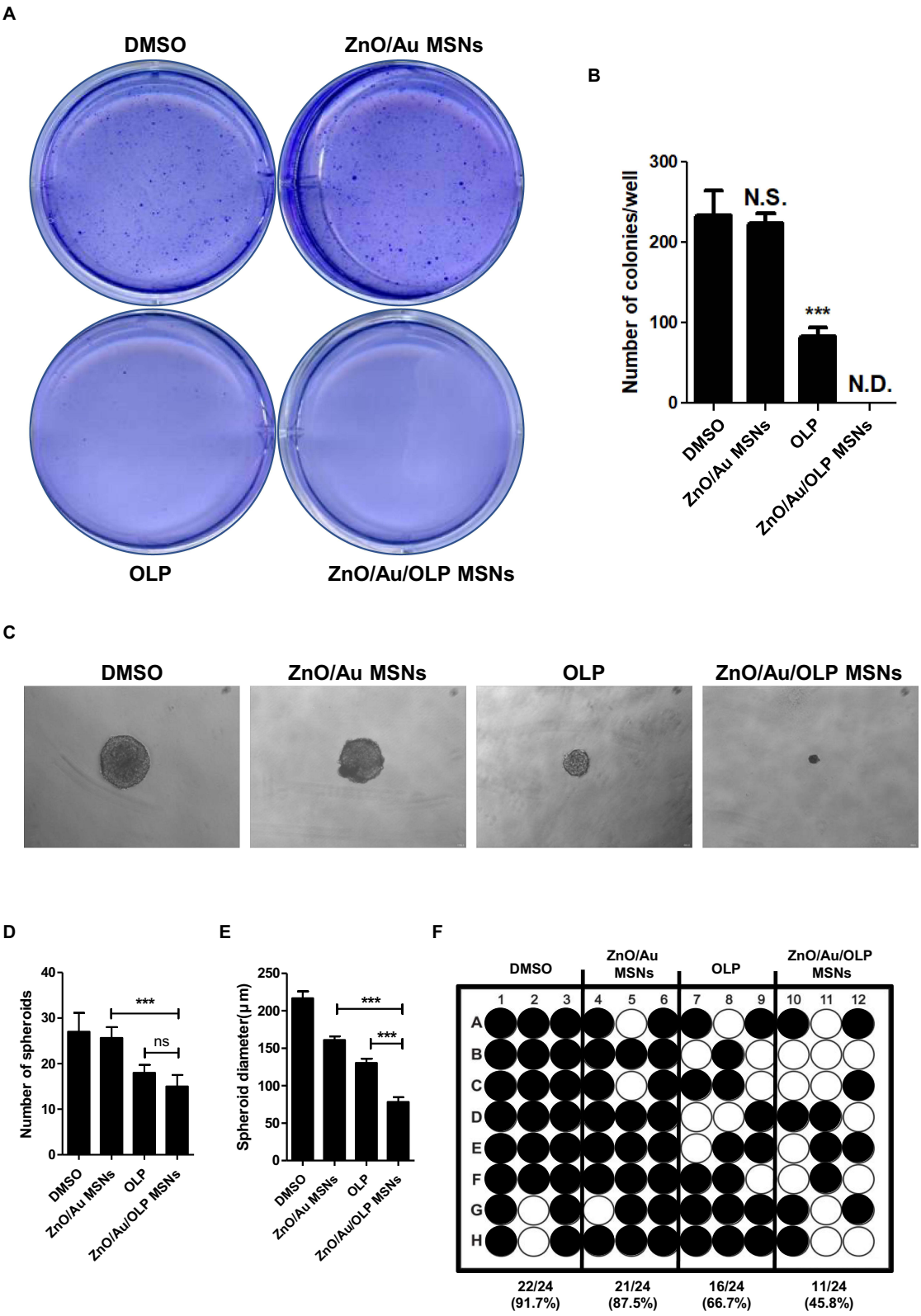

Figure 4 Colony and spheroid forming abilities decreased in ZnO/Au/OLP MSN-treated 5-FU-resistant CRC cell lines. (**A**) Colony formation ability decreased in OLP and ZnO/Au/OLP MSN-treated 5-FU-resistant CRC ells. (**B**) Quantification data of (**A**). (**C**) Spheroid formation ability was suppressed upon treatment with OLP and ZnO/Au/OLP MSNs. (**D** and **E**) Quantification data of (**A**). (**F**) Single cell derived spheroid formation was reduced in OLP and ZnO/Au/OLP MSNs. Values are expressed as the mean ± standard error of the mean (S.E.M). ***p < 0.001 as compared to the control group.

Abbreviation: N.S, Not specified.

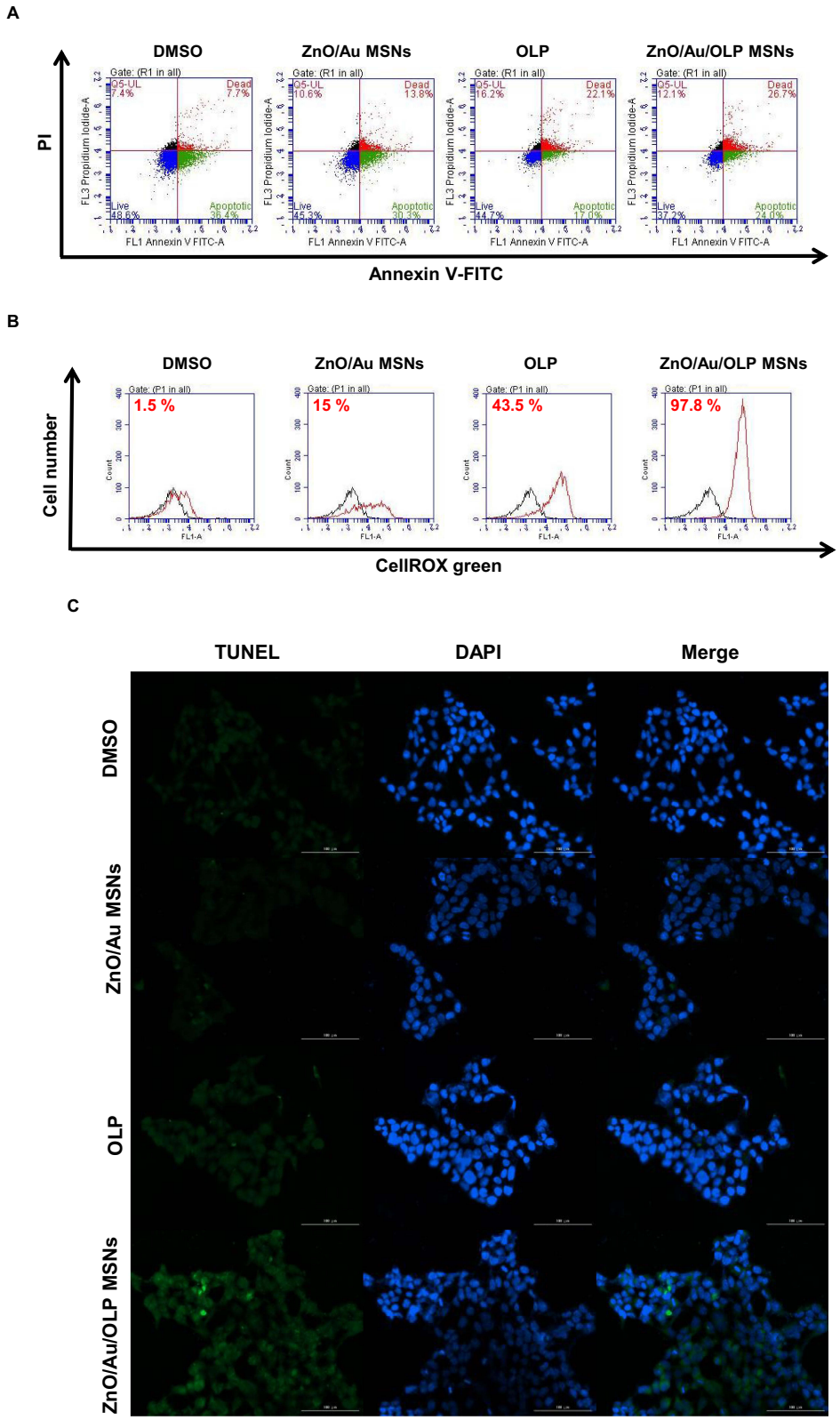

Figure 5 OLP and ZnO/Au/OLP MSNs induced late phase apoptosis in 5-FU-resistant CRC cells. (**A**) Annexin V/propidium iodide-labeled apoptotic 5-FU-resistant CRC cells were detected using flow cytometry. (**B**) CellROX staining was detected using FACS displaying the production of intracellular ROS. (**C**) TUNEL staining for the assessment of apoptosis in 5-FU-resistant CRC cells.

3-fold higher compared to the control group treated with DMSO. Reactive oxygen species (ROS) and mitochondria in the apoptosis process (Figure 5B). ROS accumulation was assessed using CellROX staining coupled with flow cytometry analysis. This assessment revealed a significant increase in intracellular ROS accumulation in cells treated with ZnO/Au/OLP MSNs compared to those treated with OLP alone.

Furthermore, Figure 5C illustrates that the increased intracellular ROS is associated with mitochondrial depolarization, as evidenced by JC-1 staining. This mitochondrial dysfunction is a key factor contributing to the late phase of apoptosis, primarily caused by DNA damage, which was confirmed by TUNEL assay.

Investigating Mitochondrial Dysfunction and Apoptosis Induction in 5-FU-Resistant CRC Cells Treated with ZnO/Au/OLP MSNs

In our study, the intensity of JC-1 green fluorescence revealed a loss of mitochondrial membrane potential (ΔΨm), indicating mitochondrial damage. This damage was specifically observed in cells treated with ZnO/Au/OLP MSNs, whereas cells treated with OLP did not show such effects (Figure 6A). In contrast, cells treated with OLP did not exhibit such effects. The loss of ΔΨm, a marker of mitochondrial dysfunction, is commonly associated with the production of reactive oxygen species (ROS). Following the treatment with ZnO/Au/OLP MSNs, there was a significant upregulation in the expression of pro-apoptotic proteins, including BAX and NIX, as indicated in Figure 6B. These findings indicate that the ZnO/Au/OLP MSNs facilitate upregulation of intracellular ROS, which in turn induces mitochondrial dysfunction and the induction of apoptosis.

Discussion

5-FU is one of the primary chemotherapeutic agents for patients with CRC.[23,24] However, its treatment is associated with various side effects[3,25,26] and drug resistance.[27–29] To overcome 5-FU-resistance in CRC, the combinations of chemotherapy[30,31] and immunotherapy[32,33] are generally used. However, combination chemotherapy such as "FOLFOX" or 'FOLFIRI'[34] and immunotherapy such as pembrolizumab[35] or nivolizumab[36] cannot completely cure patients with CRC. Thus, new strategies for the treatment of 5-FU-resistant CRC are urgently required.

Recent studies have demonstrated the anti-cancer effects of oleuropein (OLP).[13,37,38] OLP, a natural anticancer agent with high stability[39] and compromised bioavailability,[40] has been successfully formulated in ZnO/Au MSNs. However, no studies have confirmed the effect of OLP-loaded nanoparticles on anti-5-FU-resistant cancer cells. Therefore, the present study validated the anti-5-FU-resistant cancer effects of ZnO/Au/OLP MSNs, especially on 5-FU-resistant DLD-1 cells in vitro. The characteristics of the ZnO/Au/OLP MSNs were examined by TEM imaging, EDS analysis, UV-visible and NIR spectrometry, and dynamic light scattering (DLS) analysis.

Spherical AuNPs with a localized SPR band around 520 nm are ideal photothermal agents for biomedical applications because they are non-toxic.[41,42] Moreover, the study confirmed the biocompatibility of ZnO/Au MSNs using CCK-8 assays. These data confirmed that the ZnO/Au/OLP MSNs effectively reduced cell viability and proliferation. Although the ZnO/Au/OLP MSNs loaded level was approximately 2.5-fold lower than that of OLP, it induced more damage to 5-FU-resistant DLD-1 cells. Additionally, it was confirmed that cell functions, including migration, invasion, and colony- and spheroid-forming abilities, were significantly reduced in 5-FU-resistant CRC cells treated with ZnO/Au/OLP MSNs compared to those in cells treated with OLP alone.

This study clearly showed that ZnO/Au/OLP MSNs dramatically induced cell death in 5-FU-resistant CRC cells. We also assessed the increased late apoptosis levels in the ZnO/Au/OLP MSNs via Annexin V/PI staining and flow cytometry. Moreover, apoptosis has been correlated with loss of MMP and ROS accumulation in previous studies.[43] Therefore, ROS accumulation and MMP loss via ROX green and JC-1 staining were confirmed in the present study. BNIP3L/NIX is a mitochondrial membrane protein that increases proapoptotic protein BAX expression.[44] BAX induces apoptosis in cancer cells.[45–47] The protein levels of BNIP3L/NIX and BAX increased in a dose-dependent manner after OLP treatment; however, this increase was more pronounced after ZnO/Au/OLP MSN treatment, as shown by Western blotting results. In summary, anti-5-FU-resistant CRC effects were demonstrated in this study. These data showed that ZnO/Au/OLP MSNs induced the accumulation of intracellular ROS and mitochondrial damage. This induced DNA

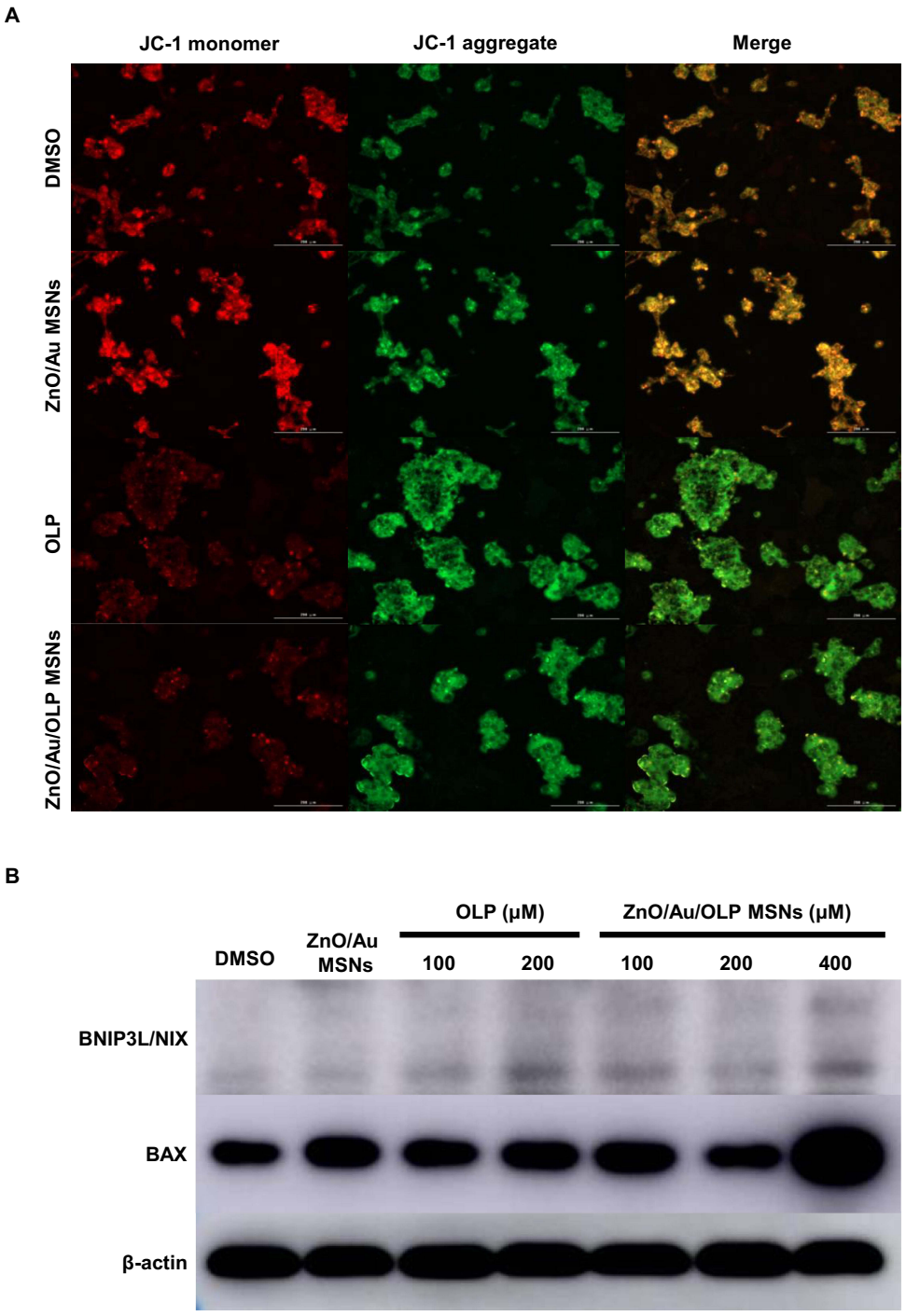

Figure 6 OLP and ZnO/Au/OLP MSNs induced 5-FU resistant cancer cells' apoptosis via loss of mitochondrial membrane potential. (**A**) JC-1 staining to evaluate changes in the mitochondria membrane potential. In JC-1 stained cells, red fluorescence was visible in cellular areas with high mitochondrial membrane potential, whereas green fluorescence of JC-1 monomer was present in cellular areas with low mitochondrial potential. (**B**) ZnO/Au/OLP MSN-induced changes in BNIP3L/NIX and BAX protein expression were assessed using Western blotting.

damage is associated with the late phases of apoptosis and necrosis. Thus, ZnO/Au/OLP MSNs may serve as a novel therapy for patients with 5-FU-resistant CRC. Moreover, these results suggest the possibility of using ZnO/Au MSNs as an effective drug delivery system in patients with 5-FU-resistant CRC.

However, it also revealed several limitations. Firstly, the results are based primarily on in vitro experiments using 5-FU-resistant DLD-1 cells, which may not fully represent the complex interactions in an in vivo environment. The

efficacy and safety of ZnO/Au/OLP MSNs in a live organism, particularly regarding biodistribution, metabolism, and potential systemic toxicity, remain to be established. Additionally, the specific molecular mechanisms underlying the observed anti-cancer effects of ZnO/Au/OLP MSNs are not completely understood Further molecular studies are required to elucidate these mechanisms, Moreover, challenges related to the penetration depth of visible and NIR light in biological tissues and potential nanoparticle aggregation on photothermal therapy with ZnO/Au MSNs need to be addressed in future studies. These limitations highlight the need for additional research, including in vivo studies and highlight the need for additional investigations, to fully harness the potential of ZnO/Au/OLP MSNs as a novel therapeutic option for 5-FU-resistant CRC.

In conclusion, while the chemo-PTT combination therapy using ZnO/Au/OLP MSNs holds promise for treating 5-FU-resistant CRC, further research is required to validate these findings and overcome the current limitations.

In conclusion, while the chemo-photothermal therapy (PTT) combination using ZnO/Au/OLP MSNs shows promise for treating 5-FU-resistant CRC, further research is necessary to substantiate these findings and address the current limitations. Specifically, the in vitro results presented in this study would be significantly enhanced by future investigations incorporating immunohistochemistry to detect biomarkers associated with the anti-tumor efficacy of ZnO/Au/OLP MSNs. This approach would facilitate the localization and quantification of these biomarkers within tissue samples, thus providing a more detailed understanding of the cellular mechanisms involved. Such studies could offer valuable morphological correlations to complement our Western blot analyses, bridging the gap between in vitro efficacy and clinical applicability. A comprehensive evaluation of ZnO/Au/OLP MSNs, including in vivo analyses, will be crucial for advancing this novel therapeutic strategy for 5-FU-resistant CRC.

Conclusion

In this study, we found that ZnO/Au/OLP Mesoporous Silica Nanoparticles (MSNs) play a pivotal role in inducing late-phase of apoptosis in 5-FU-resistant colorectal cancer (CRC) cells. This apoptosis is primarily driven by the upregulation of intracellular reactive oxygen species (ROS) and consequent mitochondrial dysfunction, leading to DNA damage. As a result, there was a marked reduction in several key functions of 5-FU-resistant CRC cells, including proliferation, migration, invasion, and anchorage-independent growth. Notably, our finding also revealed that ZnO/Au/OLP MSNs effectively diminished the cancer stem cell (CSC) capabilities of these resistant cells.

These outcomes underscores the potential of ZnO/Au/OLP MSNs as a novel and effective approach for the treatment of 5-FU-resistant colorectal cancer. By targeting the underlying mechanisms of resistance and cancer cell survival, ZnO/Au/OLP MSNs offer a promising avenue for overcoming the limitations of current CRC therapies, paving the way for more effective and targeted treatment strategies.

Funding

This research was supported by a grant from the National Research Foundation of Korea (NRF) funded by the Republic of Korea Government (Grant No. NRF2020R1A2C2101297), and the Medical Research Center (MRC) program through the NRF, funded by the Republic of Korea Government (Grant No.2022R1A5A2027161).

Disclosure

The authors report no conflicts of interest in this work.

References

1. Biller LH, Schrag D. Diagnosis and treatment of metastatic colorectal cancer. *JAMA*. 2021;325(7):669–685. doi:10.1001/jama.2021.0106
2. KulmiraNurgali RTJ. Raquel abalo, adverse effects of cancer chemotherapy: anything new to improve tolerance and reduce sequelae? *Front Pharmacol*. 2018;9:245.
3. Shahrokni A, Reza Rajebi M, Saif MW. Toxicity and efficacy of 5-fluorouracil and capecitabine in a patient with TYMS gene polymorphism: a challenge or a dilemma? *Clin Colorectal Cancer*. 2009;8(4):231–234. doi:10.3816/CCC.2009.n.039
4. Tzekaki EE, Geromichalos G, Lavrentiadou SN, Tsantarliotou MP, Pantazaki AA, Papaspyropoulos A. Oleuropein is a natural inhibitor of PAI-1-mediated proliferation in human ER-/PR- breast cancer cells. *Breast Cancer Res Treat*. 2021;186(2):305–316. doi:10.1007/s10549-020-06054-x
5. Mohammed M.H.Al-Gayyar IOS, Al-Gayyar MMH. Oleuropein potentiates anti-tumor activity of cisplatin against HepG2 through affecting proNGF/NGF balance. *Life Sci*. 2018;198:87–93. doi:10.1016/j.lfs.2018.02.027

6. Cárdeno A, Marina Sánchez-Hidalgo MAR, Rosillo MA, de la Lastra CA. Oleuropein, a secoiridoid derived from olive tree, inhibits the proliferation of human colorectal cancer cell through downregulation of HIF-1α. *Nutr Cancer*. 2013;65(1):147–156. doi:10.1080/01635581.2013.741758
7. Elisa Giner MCR, Jose Luis R, Miguel Cerd J, Mar Giner R, Giner RM. Chemopreventive effect of oleuropein in colitis-associated colorectal cancer in c57bl/6 mice. *Mol Nutr Food Res*. 2016;60(2):242–255. doi:10.1002/mnfr.201500605
8. Yan C-M, Chai E-Q, Cai H-Y, Miao G-Y, Ma W. Oleuropein induces apoptosis via activation of caspases and suppression of phosphatidylinositol 3-kinase/protein kinase B pathway in HepG2 human hepatoma cell line. *Mol Med Rep*. 2015;11(6):4617–4624. doi:10.3892/mmr.2015.3266
9. Bulotta S, Corradino R, MarilenaCelano JM, et al. Antioxidant and antigrowth action of peracetylated oleuropein in thyroid cancer cells. *J Mol Endocrinol*. 2013;51(1):181–189.
10. Masre SF. Oleuropein and skin cancer. In: *Olives and Olive Oil in Health and Disease Prevention*. Academic Press; 2021:615–623.
11. Antognelli C, Frosini R, Santolla MF, Peirce MJ, Talesa VN. Oleuropein-induced apoptosis is mediated by mitochondrial glyoxalase 2 in NSCLC A549 cells: a mechanistic inside and a possible novel nonenzymatic role for an ancient enzyme. *Oxid Med Cell Longev*. 2019;2019.
12. Hashemi Sheikhshabani S, Amini-Farsani Z, ShimaRahmati AJ, Mohammadi-Samani M, Mohammadi-Samani M, Asgharzade S. Oleuropein reduces cisplatin resistance in ovarian cancer by targeting apoptotic pathway regulators. *Life Sci*. 2021;278:119525. doi:10.1016/j.lfs.2021.119525
13. Ruzzolini J, Peppicelli S, Andreucci E, et al. Oleuropein, the main polyphenol of Olea europaea leaf extract, has an anti-cancer effect on human braf melanoma cells and potentiates the cytotoxicity of current chemotherapies. *Nutrients*. 2018;10(12):1950. doi:10.3390/nu10121950
14. Menendez JA, Vazquez-Martin A, Colomer R, et al. Olive oil's bitter principle reverses acquired autoresistance to trastuzumab (Herceptin™) in HER2-overexpressing breast cancer cells. *BMC Cancer*. 2007;7(1):80. doi:10.1186/1471-2407-7-80
15. Kim DY, Park S, Yun J, Jang W, Rethineswaran VK, Van LT, Giang LT, Choi J, Lim HJ, Kwon SM. Oleuropein induces apoptosis in colorectal tumor spheres via mitochondrial fission. *Mol Cellular Toxicol*. 2022;19(2):2092–8467.
16. Lu J, Liong M, Li Z, Zink JI, Tamanoi F. Biodistribution, and drug-delivery efficiency of mesoporous silica nanoparticles for cancer therapy in animals. *Small*. 2010;6(16):1794–1805. doi:10.1002/smll.201000538
17. Zhang Q, Liu F, TrucNguyen K, et al. Multifunctional mesoporous silica nanoparticles for cancer-targeted and controlled drug delivery. *Adv Funct Mater*. 2012;22(24):5144–5156. doi:10.1002/adfm.201201316
18. Li T, Shi S, Goel S, Shen X, Xie X, Chen Z, Zhang H, Li S, Qin X, Yang H, Wu C. Recent advancements in mesoporous silica nanoparticles towards therapeutic applications for cancer. *Acta Biomater*. 2019;89:1–3.
19. De Luca R, Profita G, Cicero G. Nab-paclitaxel in pretreated metastatic breast cancer: evaluation of activity, safety, and quality of life. *Onco Targets Therapy*. 2019;12:1621.
20. Chen S, Greasley SL, Ong ZY. Biodegradable zinc-containing mesoporous silica nanoparticles for cancer therapy. *Mater Today Adv*. 2020;6:100066. doi:10.1016/j.mtadv.2020.100066
21. Qiao Z-A, Zhang L, Guo M, Liu Y, Huo Q. Synthesis of mesoporous silica nanoparticles via controlled hydrolysis and condensation of silicon alkoxide. *Chem Mater*. 2009;21(16):3823–3829. doi:10.1021/cm901335k
22. Ali A, Saeed S, Hussain R, et al. Synthesis and characterization of silica, silver-silica, and zinc oxide-silica nanoparticles for evaluation of blood biochemistry, oxidative stress, and hepatotoxicity in albino rats. *ACS Omega*. 2023;8(23):20900–20911. doi:10.1021/acsomega.3c01674
23. Longley DB, Paul Harkin D, Johnston PG. 5-Fluorouracil: mechanisms of action and clinical strategies. *Nat Rev Cancer*. 2003;3(5):330–338. doi:10.1038/nrc1074
24. Ghafouri-Fard S, Abak A, Tondro Anamag F, et al. 5-Fluorouracil: a narrative review on the role of regulatory mechanisms in driving resistance to this chemotherapeutic agent. *Front Oncol*. 2021;11:658636. doi:10.3389/fonc.2021.658636
25. Joon Kwon S. Management of side effects of 5-FU based chemotherapy. *Korean J Clin Oncol*. 2005;1(1):51–58.
26. Cheung WY, Fralick RA, Cheng S. The confused cancer patient: a case of 5-fluorouracil– induced encephalopathy. *Current Oncol*. 2008;15(5):234–236.
27. Blondy S, David V, Verdier M, Mathonnet M, Perraud A, Christou N.5-Fluorouracil resistance mechanisms in colorectal cancer: from classical pathways to promising processes. *Cancer Sci*. 2020;111(9):3142–3154. doi:10.1111/cas.14532
28. Zhang N, Yin Y, Sheng-Jie X, Chen W-S. 5-Fluorouracil: mechanisms of resistance and reversal strategies. *Molecules*. 2008;13(8):1551–1569. doi:10.3390/molecules13081551
29. Lingfeng H, Zhu H, Zhou S, et al. Wnt pathway is involved in 5-FU drug resistance of colorectal cancer cells. *Exp Mol Med*. 2018;50:1–12.
30. Lin C-Y, Lin T-H, Chen -C-C, Chen M-C, Chen C-P. Combination chemotherapy with Regorafenib in metastatic colorectal cancer treatment: a single center, retrospective study. *PLoS One*. 2018;13(1):e0190497. doi:10.1371/journal.pone.0190497
31. Cunningham D, Sirohi B, Pluzanska A, et al. Two different first-line 5-fluorouracil regimens with or without oxaliplatin in patients with metastatic colorectal cancer. *Ann Oncol*. 2009;20(2):244–250. doi:10.1093/annonc/mdn638
32. Weng J, Shanbao L, Zhu Z, et al. Exploring immunotherapy in colorectal cancer. *J Hematol Oncol*. 2022;15(1). doi:10.1186/s13045-022-01294-4
33. Ooki A, Shinozaki E, Yamaguchi K. Immunotherapy in colorectal cancer: current and future strategies. *J Anus Rectum Colon*. 2021;5(1):11–24. doi:10.23922/jarc.2020-064
34. Neugut AI, Lin A, Raab GT, et al. FOLFOX and FOLFIRI use in stage iv colon cancer: analysis of SEER-medicare data. *Clin Colorectal Cancer*. 2019;18(2):133–140.
35. Wookey V, Grothey A. Update on the role of pembrolizumab in patients with unresectable or metastatic colorectal cancer. *Therap Adv Gastroenterol*. 2021;14:17562848211024460. doi:10.1177/17562848211024460
36. Lenz H-J, Van Cutsem E, Luisa Limon M, et al. First-line nivolumab plus low-dose ipilimumab for microsatellite instability-high/mismatch repair-deficient metastatic colorectal cancer: the phase II checkmate 142 study. *J Clin Oncol*. 2022;40(2):161–170. doi:10.1200/JCO.21.01015
37. Ahmad Farooqi A, Fayyaz S, Sanches Silva A, et al. Oleuropein and cancer chemoprevention. *Molecules*. 2017;22(5):705. doi:10.3390/molecules22050705
38. Al-Karaki R, Awadallah A, Tawfeek&Maha Nasr HM. Preparation, characterization and cytotoxic activity of new oleuropein microemulsion against HCT-116. *Colon Cancer Cell Pharmaceutical Chem J*. 2020;53:1118–1121.
39. Markopoulos C, Vertzoni M, Agalias A, Magiatis P, Reppas C. Stability of oleuropein in the human proximal gut. *J Pharm Pharmacol*. 2009;61(2):143–149. doi:10.1211/jpp.61.02.0002

40. Huguet-Casquero A, Moreno-Sastre M, Belén López-Méndez T, Gainza E, Luis Pedraz J. Encapsulation of oleuropein in nanostructured lipid carriers: biocompatibility and antioxidant efficacy in lung epithelial cells. *Pharmaceutics*. 2020;12(5):429. doi:10.3390/pharmaceutics12050429
41. Conde J, Larguinho M, Cordeiro A, et al. Gold-nanobeacons for gene therapy: evaluation of genotoxicity, cell toxicity and proteome profiling analysis. *Nanotoxicology*. 2014;8(5):521–532. doi:10.3109/17435390.2013.802821
42. Conde J, Rosa J, Baptista P. Gold-nanobeacons as a theranostic system for the detection and inhibition of specific genes. *Protoc Exch*. 2013;1–35. doi:10.1038/protex.2013.088
43. Tang X-Q, Feng J-Q, Chen J. Protection of oxidative preconditioning against apoptosis induced by H2O2 in PC12 cells: mechanisms via MMP, ROS, and Bcl-2. *Brain Res*. 2005;1057(1–2):57–64. doi:10.1016/j.brainres.2005.07.072
44. Yue L, Zheng W, Yangyang L, et al. BNIP3L/NIX-mediated mitophagy: molecular mechanisms and implications for human disease. *Cell Death Dis*. 2022;13(1):14.
45. O'Neill KL, Huang K, Zhang J, Chen Y, Luo X. Inactivation of prosurvival Bcl-2 proteins activates Bax/Bak through the outer mitochondrial membrane. *Genes Dev*. 2016;30:1–16.
46. Lee a H-Y, Oh b S-H. Arsenite-induced cytotoxicity is regulated by p38-SQSTM1/p62 and JNK-BNIP3L/Nix signaling in lung cancer cells. *Biochem Biophys Res Commun*. 2022;587:16–23. doi:10.1016/j.bbrc.2021.11.068
47. Zhang J, Ney PA. Role of BNIP3 and NIX in cell death, autophagy, and mitophagy. *Cell Death Differ*. 2009;16(7):939–946. doi:10.1038/cdd.2009.16